Communications
doi.org/10.1002/batt.202100053

Check for updates

Chemistry Europe
European Chemical Societies Publishing

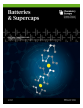

Controlling the Formation of Sodium/Black Phosphorus IntercalationCompounds Towards High Sodium Content

Katharina Werbach,*[a] Christian Neiss,[b] Alexander Müllner,[a] Gonzalo Abellán,[c] Daria Setman,[a] Vicent Lloret,[d] Stefan Wild,[d] Frank Hauke,[d] Thomas Pichler,[a] Andreas Hirsch,[d] and Herwig Peterlik[a]

The solid-state synthesis of pure sodium-black phosphorus intercalation compounds (Na-BPICs) has been optimized in bulk for two stoichiometric ratios. Specifically, *in-situ* X-Ray diffraction (XRD) allowed the precise identification of the optimal temperature range for the formation of Na-BPICs: 94 °C–96 °C. Moreover, as the undesired formation of Na_3P takes place at this very same range, we succeeded in introducing a new synthetic route based on a fast-thermal ball milling implementation that results in the bulk production of BPIC without Na_3P in 9 out of 10 cases. Finally, by combining XRD, Raman spectroscopy, and DFT calculations we developed a new structural model for Na-based BPICs showing an increase of BP's unit cell with Na atoms incorporated in every second layer. These results will pave the way for the large-scale synthesis and application of pure BPICs, which are of great interest in fields such as optoelectronics or energy storage.

The total gross electricity production worldwide has risen from ~6,500 TWh in 1975 to ~26,500 TWh in 2018[1] with no indication of a change in trend. The increasing share of renewable sources in the total energy supply,[1,2] portable consumer electronics, and – more recently – the growing use of electric cars[3] have led to an effort in R&D of batteries, primarily focused on lithium-ion batteries (LIB).[4–6] However, the predicted annual demand for lithium for electric vehicle batteries in 2030 alone surpasses the current supply by almost a factor of 2.5,[7] thus making the search for alternative materials worthwhile. Sodium-ion batteries (SIB) offer a higher energy density than aqueous batteries and a lower cost than LIB and have been the subject of research since the 1980s.[8–10] One of the challenges is to find a suitable anode material, as graphite – used in LIB – does not form stable intercalation compounds with sodium effortlessly.[10–13] Among its many unique properties, a high carrier mobility[14,15] and a high theoretical specific capacity[16,17] render black phosphorus (BP) a promising candidate. BP was proposed to be used directly in LIB[18–22] and was successfully implemented – alone, or together with graphene – as an electrode in SIB.[23–25] In its standard configuration, BP has an orthorhombic structure (Cmce, space group 64) with $a = 3.3133$ Å, $b = 10.4730$ Å, and $c = 4.3740$ Å in which the layers of phosphorene are stacked in an ABAB order along the b-axis.[26] Although only recently,[27] the intercalation of BP with sodium has been explored in a theoretical[28,29] as well as practical[30–32] manner. Depending on the amount of the intercalating atoms, the way of synthesis, and the scale of the experiment, the exact results vary: Cheng et al.,[30] performing small-scale experiments inside an HRTEM, report a stretch of ~25% in the long axis compared to pure BP, while we[32] observed an increase of ~10% in the long axis after solid-state synthesis in bulk. In the following, we analyze the sodiation process of the solid-state synthesis and the structure of the resulting intercalated BP/sodium phase. By synthesizing the intercalated phase (BPIC) *in-situ* from BP and Na in bulk, we establish the relevant parameters that lead to a successful sodiation. These will then be employed to find a suitable synthesis procedure for its larger-scale production, thus allowing a better understanding of the structure of this component.

In-Situ Synthesis

Firstly, following our previous synthetic protocol,[32,33] pure materials were placed together inside glass capillaries to follow the reaction of BP and Na *in-situ*. Due to the air-sensitivity of both components, specimens were prepared inside an argon-filled glovebox (< 10 ppm O_2 and H_2O) at standard conditions. BP crystals (99.998% purity) were ground to a fine powder in an agate mortar and placed together with an average of 1 mg Na inside a 1.5 mm diameter glass capillary in stoichiometric ratios of Na:P = 1:4 and Na:P = 1:2, respectively. Capillaries were hermetically sealed and transferred to a heating stage (Figure 1) inside a laboratory microfocus X-ray device in

[a] K. Werbach, A. Müllner, Dr. D. Setman, Prof. T. Pichler, Prof. H. Peterlik
Faculty for Physics, University of Vienna
Boltzmanngasse 5, 1090 Vienna, Austria
E-mail: katharina.werbach@univie.ac.at
[b] Dr. C. Neiss
Lehrstuhl für Theoretische Chemie,
Friedrich-Alexander-Universität Erlangen-Nürnberg (FAU)
Egerlandstrasse 3, 91058 Erlangen, Germany
[c] Dr. G. Abellán
Instituto de Ciencia Molecular (ICMol), Universidad de Valencia
Catedrático José Beltrán Martínez, 2, 46980 Paterna, Valencia, Spain
[d] V. Lloret, S. Wild, Dr. F. Hauke, Prof. A. Hirsch
Chair of Organic Chemistry II and Joint Institute of Advanced Materials and Processes (ZMP)
Friedrich-Alexander-Universität Erlangen-Nürnberg (FAU)
Nikolaus-Fiebiger-Str. 10, 91058 Erlangen, Germany

Supporting information for this article is available on the WWW under https://doi.org/10.1002/batt.202100053

© 2021 The Authors. Batteries & Supercaps published by Wiley-VCH GmbH. This is an open access article under the terms of the Creative Commons Attribution License, which permits use, distribution and reproduction in any medium, provided the original work is properly cited.

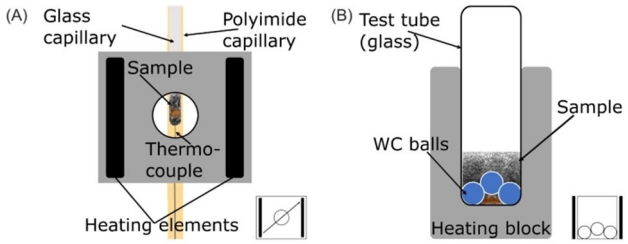

Figure 1. Schematics of experimental setups for the sodium intercalation of BP as well as their symbols displayed at their bottom-right corner: A) Furnace used for *in-situ* experiments. Sealed capillaries were held in place together with a thermocouple with the help of a polyimide capillary. Specimens were heated in steps of 10 °C. B) Ball milling was performed with 3 tungsten carbide (WC) balls that were placed together with BP and Na inside a glass test tube. Heating was performed either in steps of 10 °C or directly to a chosen temperature.

vacuum (see Supporting Information, section SI2). The temperature of the heating stage was raised from room temperature to a maximum of 220 °C in steps of 10 °C. The temperature at the capillary was recorded with a thermocouple. After every heating step – and again after cooling to room temperature – a XRD pattern was recorded from $2\theta = 5°$ to $2\theta = 30°$. Whenever possible, XRD pattern up to $2\theta = 60°$ were recorded afterward. In total, we evaluated 22 specimens, 11 of each stoichiometric composition.

In all specimens, BP and Na were identified as separate phases at room temperature. Upon heating, the Na peak vanishes after the specimens are heated to ~90 °C. Upon heating further, in some cases the temperature measurement curve shows a strong divergence at (94 ± 2) °C for specimens mixed in the stoichiometric ratio of Na:P = 1:4 and at (97 ± 2) °C for ones mixed in the stoichiometric ratio of Na:P = 1:2, respectively. The comparatively large temperature error is estimated, as the thermocouple is located outside the capillary, but in close contact (see Figure 1). This is accompanied by the appearance of new peaks in the recorded XRD patterns and indicates an exothermic reaction. Nine glass capillaries broke during heat treatment or were damaged severely enough to break after removing them from the heating stage. While it cannot be completely ruled out that this affects the synthesis, since the measurements were performed in vacuum and the stabilizing polyimide capillary (Figure 1) always remained intact, we included these results in the evaluation. Optical inspection after heat treatment indicated that the reaction takes place locally for most specimens (see Supporting Information, Figure SI1.1). Re-opening one of the specimens showed a separation into a solid part and residuals of BP powder (Figure SI1.1).

Table 1. Characteristic XRD reflections in the range of 2θ up to 30° of the observed phases and their abbreviations.

Name	Characteristic XRD reflections (2θ)		
Intercalated Phase (BPIC)	14.1° (IC#1a)	15.4° (IC#1)	23.4° (IC#2)
Na_3P[34,35]	20.1°	20.7°	23.1°
Black Phosphorus (BP)[26]	16.9°		26.6°

Phase Identification

XRD patterns exhibited diffraction lines from pristine BP after heat treatment in the whole sample. Additionally, they may be classified further (Figure 2/Table 1): The intermetallic phase Na_3P could be identified by its characteristic diffraction lines at

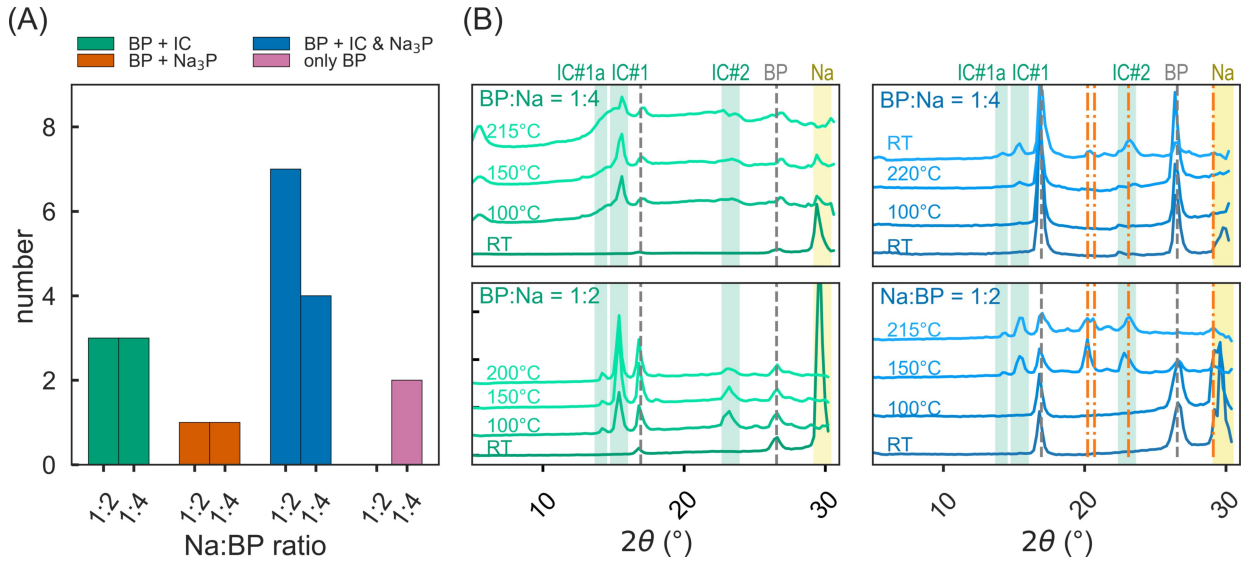

Figure 2. Results of *in-situ* experiments: A) Left side: most specimens showed a mixture of both the intercalated phase and Na_3P additionally to pure BP. Two specimens showed no reaction at all during the first heating process. B) Right side: XRD patterns were recorded at room temperature and after every heating step (exemplary shown for specimens of both compositions for four temperatures each). Green bands visualize the specific peaks at 15.4° (IC#1), 23.4° (IC#2), and 14.1° (IC#1a) which were used as an indicator for the formation of the intercalated phase and a yellow band visualizes pure sodium. The phase Na_3P (orange, dotted dashed) was also observed as the only intermetallic phase.

© 2021 The Authors. Batteries & Supercaps published by Wiley-VCH GmbH

$2\theta = 20.1°$, $2\theta = 20.7°$ and $2\theta = 23.1°$[34,35]. Two further diffraction peaks at $2\theta \sim 15.4°$ (IC#1) and $2\theta \sim 23.4°$ (IC#2) that could not be attributed to a known intermetallic phase were observed in the patterns of 18 specimens.

IC#1 was previously associated with the formation of a metal intercalated phosphorous phase,[32] further supported by the occurrence of Raman bands at ~300 cm^{-1}[32,extended data in 36]. In 15 out of the 18 cases mentioned above, another peak at $2\theta \sim 14.1°$ (IC#1a) was observed. Only a minority of specimens shows a single phase as the result of the reaction; in most cases, a mixture of different phases was observed. Due to the clear separation of the Raman bands of Na_3P and BP (see Supporting Information, section SI4, tables SI4.1 and SI4.2), Raman spectroscopy was used to identify the preferred area of reaction. The patterns show – in accordance with XRD results pure BP, but also broad bands at ~300 cm^{-1} primarily at the solid part of the specimen (Figure 3).

Concluding, IC#1 as well as the occurrence of Raman bands at ~300 cm^{-1} were used as an indicator of the successful formation of Na-black phosphorous intercalated phase (Na-BPIC).

As IC#2 occurs at angles where one of the characteristic peaks of Na_3P is also observed, the specimen is considered as one that exclusively contains BPIC and additionally BP only if reflections of Na_3P at higher diffraction angles are absent and IC#1 is present. For two specimens showing only pure BP after heat treatment (see Figure 2), re-heating lead to the emergence of the characteristic peaks IC#1 and IC#2, without traces of Na_3P. Furthermore, one specimen's temperature measurement curve exhibited a strong divergence right before the emergence of the characteristic X-ray peaks (Figure SI2.3), which led to the destruction of the capillary. Raman spectra were recorded for the other specimen again showing the characteristic bands at 300 cm^{-1} (Figure SI2.3).

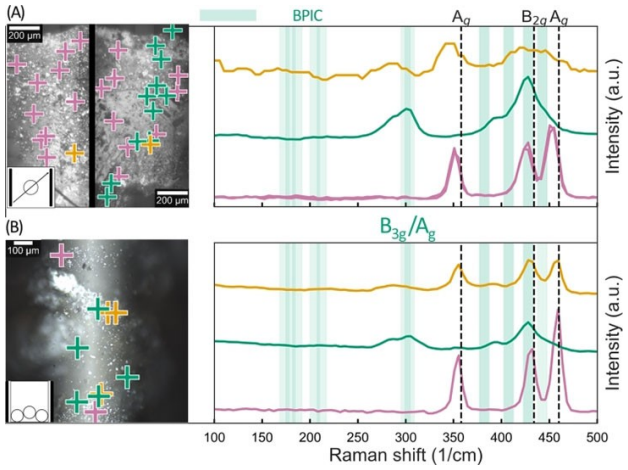

Figure 3. Raman spectra of specimens after heat treatment, both mixed with starting concentration Na:P = 1:4 Dashed black lines: pure BP. Green bands: calculated Raman active modes of BPIC. For a full list of all Raman-active modes see the Supporting Information, table SI4.4. Three types of spectra can be identified: pure BP (pink), BPIC (green), and mixed (orange), where the A_g^1 mode of BP can still be identified. A) Top row: *in-situ* specimen #29 after heat treatment up to 220 °C. The specimen was divided into two parts, one solid, the other consisting of powder. BP is dominant in the powdery part, while BPIC can be found in the solid part. B) Bottom row: ball-milled specimen LXXIX, which was directly heated up to 94 °C with 700 rpm and annealed for 1 min. BP and BPIC are interspersed throughout the specimen.

Narrowing down the temperature range of the reaction was attempted by using differential scanning calorimetry (DSC). Specimens mixed in stoichiometric ratios Na:P = 1:4 (with 1 mg Na) and Na:P = 3:1 (with 2.7 mg Na) were heated beyond the melting point of Na with different heating rates (see section SI6). While BPIC was not formed in this way, it allowed the reaction of Na and BP to Na_3P to be specified to (97.1 ± 0.2) °C, roughly corresponding to the melting point of Na (97.7 °C) and the average reaction temperature for in-situ specimens with starting ratios of Na:P = 1:2.

Solid-state synthesis of BPIC could be followed *in-situ*: Specimens showed a variety of possible outcomes, with a localized formation of BPIC as well as Na_3P. Most likely, this stems from the method of synthesis, where Na is locally overabundant, thus facilitating the spontaneous formation of Na_3P. Also, an orientation dependence of an electrochemically driven intercalation of BP was reported,[37] which was not considered in this setup. The reaction of BP and Na to form BPIC occurs spontaneously at a temperature range between 94 °C and 97 °C, is exothermic, and possibly accompanied by a volumetric expansion (both of which may lead to the breaking of some capillaries). Capillary breakage was observed primarily in specimens where only BPIC and BP were identified, while in those with mixed phases of BPIC, BP, and Na_3P, it occurred to a lesser extent.

While the presence of Na_3P is not necessarily detrimental to intercalation – both phases may even form at the same time – it makes the determination of BPIC's structure considerably more difficult due to the overlap of characteristic XRD reflections and has an important influence on the electrochemical behavior of BP-based SIBs.[23] Thus, the suppression of Na_3P is a matter of utmost importance.

Ball Milling

To overcome this problem, mechanical homogenization *via* ball milling during the heating process was implemented into the synthesis procedure for the first time. As specimens with a starting ratio of Na:P = 1:2 show a stronger tendency to form Na_3P (Figure 2), only specimens with stoichiometric concentrations of Na:P = 1:4 were considered for optimization. Forty-three such specimens containing (2.8 ± 0.1) mg Na on average) were heated up and simultaneously ball-milled at 700 rpm. The previously established reaction temperature range of 94 °C–97 °C was explored by either heating in 10 °C steps like the *in-situ* experiments or by directly exposing the sample in one step to a defined temperature.

BPIC was identified with the previously established fingerprints: the presence of IC#1 and IC#2, without the characteristic Na_3P reflections in the XRD patterns, as well as the typical emergence of broad vibration bands around at ~300 cm^{-1} in the Raman spectra for selected specimens.

© 2021 The Authors. Batteries & Supercaps published by Wiley-VCH GmbH

Heating specimens to (92 ± 1) °C for 1, 3, and 5 minutes does not lead to any reaction for specimens treated in such a way, independent of the concentration of Na: Pure BP – as well as pure Na – can be observed. Heating specimens to (94 ± 1) °C and (96 ± 1) °C for 1, 3, and 5 minutes resulted in specimens showing Na_3P and/or BPIC additionally to pure BP (see Figure 4). Most of them show at least traces of Na_3P, while one specimen (XXIII) seemed only to consist of pure BP. Upon re-heating, the formation of IC#1 and IC#2 was observed (Figure SI2.2). Raman spectra of this specimen also showed the characteristic band at ~300 cm^{-1} of the *in-situ* synthesized BPIC-containing specimens. Using Raman spectroscopy again as a tool to characterize the distribution of BPIC, we find a more uniform distribution of BPIC throughout the specimen compared to the *in-situ* approach (Figure 3). Specimens mixed in ratios Na:P = 1.4 and Na:P = 3:1 heated inside the DSC following the same temperature protocol showed no reaction at all, indicating that ball-milling is essential to facilitate a reaction of BP and Na below the melting point of Na.

Interestingly, although only a minority of the synthesized specimens exclusively showed BPIC in addition to pure BP, we succeeded in establishing a novel synthesis procedure that leads to the formation of BPIC without the simultaneous formation of Na_3P: heating the raw materials directly to 94 °C for 1–3 min while ball milling reliably produces BPIC phase without Na_3P in 9 out of 10 investigated cases.

Structure of the Intercalated Phase

To gain further insight into the structure of BPIC, we carried out a theoretical study using quantum mechanical calculations. The geometries of structures for Na:P concentrations of Na:P = 1:4 and Na:P = 1:8 were modeled by placing Na atoms between every layer of BP and allowing for structural relaxation (see section SI4.1), yielding possible structures of stage 1 Na-BPICs.[32]

However, calculated Raman active frequencies of homogeneously intercalated Na-BPIC models cannot reproduce a Raman-active mode at ~300 cm^{-1} (Figure SI5.1). Therefore, it seems unlikely that BPIC observed here is identical to the calculated stage structures.

BP's (020) XRD reflection is directly related to the layer distance of individual phosphorene layers. While reflections corresponding to the layer distances of the calculated stage 1 Na-BPICs match either IC#1 or IC#1a and IC#2, measured patterns are not adequately represented by the calculated patterns (Figure SI5.1). We therefore considered inhomogeneously intercalated structures corresponding to stage 2 Na-BPICs where Na is present in only every second layer in further calculations. This induces gliding of the sodium filled BP layers away from AB to a slightly distorted AC or AD stacking (due to the distortion AC and AD are not strictly defined anymore) in only every second layer and a doubling of the unit cell (Figure 5). The proposed gliding of individual BP layers from their AB stacking order upon sodiation is in accordance with previous *in-situ* experimental results for a Na-BPIC synthesized in a scanning transmission electron microscope (STEM).[30]

It should be noted that the (0k0) reflections in our model now correspond to the average layer spacing and that the distances of the intercalated (ΔAC) and non-intercalated (ΔAB) layers differ significantly (see Figure 5). The stage 2 model also predicts a Raman-active mode at ~300 cm^{-1}, *i.e.* yield a match within uncertainties of the calculation for a model with a mixed stacking (Figure 3). Vibrational modes between 250 cm^{-1} and 350 cm^{-1} can be attributed to the weakening of P–P bonds that connect the zig-zag-layers of BP, which effectively leads to modes similar to the A_g^1 mode of BP at lower frequency.[32]

Comparing the XRD pattern calculated from this model to measured ones, a significant difference can be found for the (020) reflection at 2θ ~ 7°. While this reflection is expected to be visible in the calculated model, it could not be observed in the investigated specimens. Therefore, structural models of stage 2 Na-BPICs with the possibility of changing the lattice parameters as well as the phosphorene layer distance were constructed to calculate theoretical XRD reflections. Model patterns were

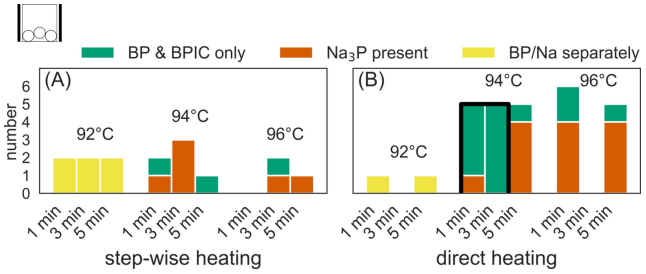

Figure 4. Outcomes of ball milling procedures. A) Left side: Stepwise heating analogous to the *in-situ* experiments. At 92 °C, both BP and Na appear as separate phases. Higher temperatures yield mixed results, additionally to pure BP Na_3P could be identified. B) Right side: Direct heating to a defined temperature. Short homogenization times at 94 °C leads to the best results (i.e. pure BPIC in addition to remaining BP in 9 out of 10 investigated cases), while Na_3P could be identified in specimens that were ball-milled longer and/or at higher temperatures.

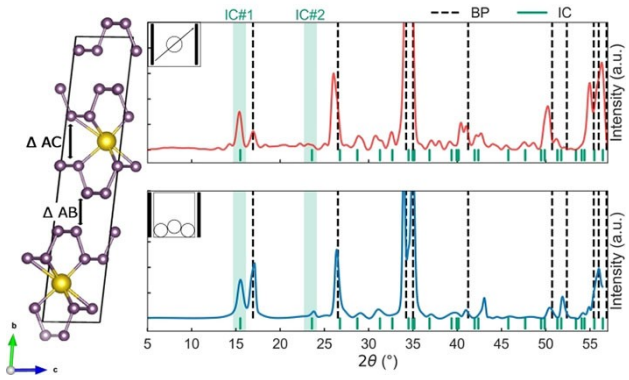

Figure 5. Calculated and measured XRD patterns for the proposed model (left) of intercalation with $a = 3.25$ Å, $b = 23.09$ Å, $c = 4.54$ Å, $\alpha = 85.5°$, $\beta = \gamma = 90°$. AB distance set to be equal to pure BP, AC distance 4.1 Å. Intercalated phase indicated by green bars. Dashed black lines: pure BP reflections. Top row: *in-situ* specimen #12. Bottom row: ball-milled specimen XXIII, heated stepwise to 94 °C for 1 min (for nomenclature see SI.1.3). Both specimens with starting ratio of Na:P = 1:4. Structure visualized with VESTA3.5.2.[38]

© 2021 The Authors. Batteries & Supercaps published by Wiley-VCH GmbH

compared to measured XRD patterns from $2\theta = 5°$ to $2\theta = 60°$. Of all patterns from ball-milled and *in-situ* specimens we selected those that showed only the BPIC (and pure BP) but no traces of Na_3P. Each was evaluated individually for the best matching parameters of BPIC, yielding a monoclinic lattice with parameters $a = 3.30$ Å, $b = 23.04$ Å, $c = 4.54$ Å, and $\alpha = 85.5° \; \gamma = \beta = 90°$ on average, which correspond well with the results of the DFT calculations (Figure SI5.2).

We also found that the visibility of BPIC's (020) reflection at $2\theta \sim 7°$ depends on two factors: the distance of the not-intercalated layers and the Na occupancy of the intercalated layer. If the distance of the non-intercalated layers widens and Na positions of the intercalated layers are fully occupied, this reflection vanishes (Figure SI5.3). As we do not observe the (020) reflection, we conclude that this is the case in our specimens.

While such a model explains the main observed features in both structural analysis methods, the small – but clearly distinguishable – peak IC#1a at $2\theta = 14°$ is still unaccounted for. However, reconsidering stage 1 intercalated structures, calculations show the appearance of peak IC#1a for models with Na : P = 1 : 8 (Figure SI5.4).

Therefore, we tentatively assign IC#1a to a stage 1 BPIC, also occurring in small amounts in some of our specimens. This suggests that the process of intercalation of BP may occur similarly to that of the well-investigated graphite intercalation compounds[12]: at first filling every second layer and subsequently filling up the remaining layers.

A comparison of the three presented synthesis methods – during DSC, via heating of reagents in a small glass capillary, and by means of ball mill-assisted heating – reveals major differences in the success of BPIC production: while BPIC is not found in the samples prepared during DSC, it appears in the samples prepared by the other two methods. Note that this behavior cannot be caused by the heating rate[1], which was set in DSC to match that of the other methods (Figures SI6.2 and SI6.3). The main difference is that samples in the confined space of the capillary, or even more so during ball milling, are subjected to considerable mechanical stress, which is not the case in the crucibles used for DSC (Figures SI1.1 and SI6.1). Thus, considering that ball-milling at 94 °C resulted in the least number of specimens containing Na_3P, it can be concluded that the ideal reaction conditions for producing BPIC require high pressure.

Summarizing, we identified for the first time the thermodynamically preferred range for the bulk formation of BPIC during solid-state synthesis. We also proposed a synthesis method for the creation of BPIC without intermetallic phases. Furthermore, significant progress has been made towards a precise determination of the BPIC's structure: alternating Na-filled and empty layers as well as small areas of stage 1 intercalated layers. This opens a door towards a large-scale synthesis of BPIC for practical applications and shed light on the structural behavior of Na-BPICs, one of the most promising materials for SIBs.

Supporting Information

Additional references cited with the Supporting Information[39–51].

Acknowledgments

The authors thank Stephan Loyer for technical support and Stefan Hummel for technical assistance with Raman spectroscopy. Christian Neiss thanks the Deutsche Forschungsgemeinschaft (DFG, Project number 182849149 – SFB 953) and the Interdisciplinary Center for Molecular Materials (ICMM) for financial support. This work has been supported by the European Research Council (ERC Starting grant N0. 2D-PnictoChem 804110 to G.A. and ERC Advanced Grant B-PhosphoChem 742145 to A.H.), the Spanish MICINN (PID2019-111742GA-I00 and Unit of Excellence "María de Maeztu" CEX2019-000919-M), the DFG (FLAG-ERA AB694/2-1), the Generalitat Valenciana (CIDEGENT/2018/001) and iDiFEDER/2018/061 co-financed by FEDER.

Conflict of Interest

The authors declare no conflict of interest.

Keywords: black phosphorus · DFT calculations · intercalation compounds · sodium · X-ray diffraction

[1] IEA, "Electricity Information: Overview", can be found under https://www.iea.org/reports/electricity-information-overview, **2020**.
[2] D. Jones, E. Graham, P. Tunbridge, A. Ilas, "Global Electricity Review", can be found under https://ember-climate.org/wp-content/uploads/2020/03/Ember-2020GlobalElectricityReview-Web.pdf, **2020**.
[3] IEA, "Global EV Outlook 2020", can be found under https://www.iea.org/reports/global-ev-outlook-2020, **2020**.
[4] a) P. K. Nayak, L. Yang, W. Brehm, P. Adelhelm, *Angew. Chem. Int. Ed.* **2018**, *57*, 102–120; *Angew. Chem.* **2018**, *130*, 106–126; b) *Angew. Chem.* **2018**, *130*, 106–126; *Angew. Chem. Int. Ed.* **2018**, *57*, 102–120.
[5] L. Li, Y. Yu, G. J. Ye, Q. Ge, X. Ou, H. Wu, D. Feng, X. H. Chen, Y. Zhang, *Nat. Nanotechnol.* **2014**, *9*, 372–377.
[6] C. Chowdhury, A. Datta, *J. Phys. Chem. Lett.* **2017**, *8*, 2909–2916.
[7] IEA, "Annual lithium demand for electric vehicle batteries, 2019–2030", can be found under https://www.iea.org/data-and-statistics/charts/annual-lithium-demand-for-electric-vehicle-batteries-2019-2030-2, **2020**.
[8] a) D. Kundu, E. Talaie, V. Duffort, L. F. Nazar, *Angew. Chem. Int. Ed.* **2015**, *54*, 3432–3448; b) *Angew. Chem.* **2015**, *127*, 3495–3513; *Angew. Chem. Int. Ed.* **2015**, *54*, 3431–3448.
[9] N. Yabuuchi, K. Kubota, M. Dahbi, S. Komaba, *Chem. Rev.* **2014**, *114*, 11636–11682.
[10] C. Delmas, *Adv. Energy Mater.* **2018**, *8*, 1703137.
[11] H. Moriwake, A. Kuwabara, C. A. J. Fisher, Y. Ikuhara, *RSC Adv.* **2017**, *7*, 36550–36554.
[12] M. S. Dresselhaus, G. Dresselhaus, *Adv. Phys.* **2002**, *51*, 1–186.
[13] a) B. Jache, P. Adelhelm, *Angew. Chem. Int. Ed.* **2014**, *53*, 10169–10173; *Angew. Chem.* **2014**, *126*, 10333–10337; b) *Angew. Chem.* **2014**,126, 10333–10337; *Angew. Chem. Int. Ed.* **2014**, *53*, 10169–10173.
[14] H. Liu, Y. Du, Y. Deng, P. D. Ye, *Chem. Soc. Rev.* **2015**, *44*, 2732–2743.
[15] J. Qiao, X. Kong, Z. X. Hu, F. Yang, W. Ji, *Nat. Commun.* **2014**, *5*, 1–7.
[16] L. Kou, C. Chen, S. C. Smith, *J. Phys. Chem. Lett.* **2015**, *6*, 2794–2805.
[17] M. Mayo, K. J. Griffith, C. J. Pickard, A. J. Morris, *Chem. Mater.* **2016**, *28*, 2011–2021.
[18] C. M. Park, H. J. Sohn, *Adv. Mater.* **2007**, *19*, 2465–2468.

© 2021 The Authors. Batteries & Supercaps published by Wiley-VCH GmbH

[19] J. Sun, G. Zheng, H. W. Lee, N. Liu, H. Wang, H. Yao, W. Yang, Y. Cui, *Nano Lett.* **2014**, *14*, 4573–4580.
[20] L. Chen, G. Zhou, Z. Liu, X. Ma, J. Chen, Z. Zhang, X. Ma, F. Li, H. M. Cheng, W. Ren, *Adv. Mater.* **2016**, *28*, 510–517.
[21] G. C. Guo, D. Wang, X. L. Wei, Q. Zhang, H. Liu, W. M. Lau, L. M. Liu, *J. Phys. Chem. Lett.* **2015**, *6*, 5002–5008.
[22] H. Jin, S. Xin, C. Chuang, W. Li, H. Wang, J. Zhu, H. Xie, T. Zhang, Y. Wan, Z. Qi, W. Yan, Y.-R. Lu, T.-S. Chan, X. Wu, J. B. Goodenough, H. Ji, X. Duan, *Science* **2020**, *370*, 192–197.
[23] J. Sun, H. W. Lee, M. Pasta, H. Yuan, G. Zheng, Y. Sun, Y. Li, Y. Cui, *Nat. Nanotechnol.* **2015**, *10*, 980–985.
[24] M. Qiu, Z. T. Sun, D. K. Sang, X. G. Han, H. Zhang, C. M. Niu, *Nanoscale* **2017**, *9*, 13384–13403.
[25] R. Hultgren, N. S. Gingrich, B. E. Warren, *J. Chem. Phys.* **1935**, *3*, 351–355.
[26] L. Cartz, S. R. Srinivasa, R. J. Riedner, J. D. Jorgensen, T. G. Worlton, *J. Chem. Phys.* **1979**, *71*, 1718–1721.
[27] a) A. Hirsch, F. Hauke, *Angew. Chem. Int. Ed.* **2018**, *57*, 4338–4354; *Angew. Chem.* **2018**, *130*, 4421–4437; b) *Angew.Chem.* **2018**, *130*,4421–4437; *Angew. Chem. Int. Ed.* **2018**, *57*, 4338–4354.
[28] K. P. S. S. Hembram, H. Jung, B. C. Yeo, S. J. Pai, S. Kim, K. R. Lee, S. S. Han, *J. Phys. Chem. C* **2015**, *119*, 216–221.
[29] X. F. Yu, H. Ushiyama, K. Yamashita, *Chem. Lett.* **2014**, *43*, 1940–1942.
[30] Y. Cheng, Y. Zhu, Y. Han, Z. Liu, B. Yang, A. Nie, W. Huang, R. Shahbazian-Yassar, F. Mashayek, *Chem. Mater.* **2017**, *29*, 1350–1356.
[31] A. Nie, Y. Cheng, S. Ning, T. Foroozan, P. Yasaei, W. Li, B. Song, Y. Yuan, L. Chen, A. Salehi-Khojin, F. Mashayek, R. Shahbazian-Yassar, *Nano Lett.* **2016**, *16*, 2240–2247.
[32] a) G. Abellán, C. Neiss, V. Lloret, S. Wild, J. C. J. C. Chacón-Torres, K. Werbach, F. Fedi, H. Shiozawa, A. Görling, H. Peterlik, T. Pichler, F. Hauke, A. Hirsch, *Angew. Chem. Int. Ed.* **2017**, *56*, 15267–15273; *Angew. Chem.* **2017**, *129*, 15469–15475; b) *Angew. Chem.* **2017**, *129*, 15469–15475; *Angew. Chem. Int. Ed.* **2017**, *56*, 15267–15273.
[33] a) S. Wild, X. T. Dinh, H. Maid, F. Hauke, G. Abellán, A. Hirsch, *Angew. Chem. Int. Ed.* **2020**, *59*, 20230–20234; b) *Angew.Chem.* **2020**,*132*, 20406–20411.
[34] G. Brauer, E. Zintl, *Z. Phys. Chem.* **1937**, *37B*, 323–352.
[35] Y. Dong, F. J. Disalvo, *Acta Crystallogr. Section E* **2005**, *61*, i223–i224.
[36] M. C. Watts, L. Picco, F. S. Russell-Pavier, P. L. Cullen, T. S. Miller, S. P. Bartuś, O. D. Payton, N. T. Skipper, V. Tileli, C. A. Howard, *Nature* **2019**, 568, 216–220.
[37] S. Kim, J. Cui, V. P. Dravid, K. He, *Adv. Mater.* **2019**, *31*, 1904623.
[38] K. Momma, F. Izumi, *J. Appl. Crystallogr.* **2011**, *44*, 1272–1276.
[39] G. Kresse, J. Furthmüller, *Comput. Mater. Sci.* **1996**, *6*, 15–50.
[40] G. Kresse, J. Furthmüller, *Phys. Rev. B* **1996**, *54*, 11169–11186.
[41] P. E. Blöchl, *Phys. Rev. B* **1994**, *50*, 17953–17979.
[42] D. Joubert, *Phys. Rev. B* **1999**, *59*, 1758–1775.
[43] J. P. Perdew, K. Burke, M. Ernzerhof, *Phys. Rev. Lett.* **1996**, *77*, 3865–3868.
[44] S. Grimme, S. Ehrlich, L. Goerigk, *J. Comput. Chem.* **2011**, *32*, 1456–1465.
[45] S. Grimme, J. Antony, S. Ehrlich, H. Krieg, *J. Chem. Phys.* **2010**, *132*, 154104.
[46] M. Methfessel, A. T. Paxton, *Phys. Rev. B* **1989**, *40*, 3616–3621.
[47] H. J. Monkhorst, J. D. Pack, *Phys. Rev. B* **1976**, *13*, 5188–5192.
[48] A. Castellanos-Gomez, L. Vicarelli, E. Prada, J. O. Island, K. L. Narasimha-Acharya, S. I. Blanter, D. J. Groenendijk, M. Buscema, G. A. Steele, J. v Alvarez, H. W. Zandbergen, J. J. Palacios, H. S. J. van der Zant, *2D Mater.* **2014**, *1*, 025001.
[49] Y. Akahama, M. Kobayashi, H. Kawamura, *Solid State Commun.* **1997**, *104*, 311–315.
[50] M. Dusek, V. Petricek, *Acta Crystallogr.* **2005**, *61*, c104–c105.
[51] C. F. MacRae, I. Sovago, S. J. Cottrell, P. T. A. Galek, P. McCabe, E. Pidcock, M. Platings, G. P. Shields, J. S. Stevens, M. Towler, P. A. Wood, *J. Appl. Crystallogr.* **2020**, *53*, 226–235.

Manuscript received: February 23, 2021
Revised manuscript received: March 4, 2021
Accepted manuscript online: March 5, 2021
Version of record online: March 31, 2021

© 2021 The Authors. Batteries & Supercaps published by Wiley-VCH GmbH